HAIT Journal of Science and Engineering, Volume 1, Issue 4, pp. 673-706

Dynamic and size dependent effects in the Condon domain state

Nathan Logoboy[1,2,*], Alexander Gordon[3], and Walter Joss[1]

[1] *Grenoble High Magnetic Field Laboratory,*
Max-Planck-Institute für Festkörperforschung and CNRS,
25 Avenue des Martyrs, BP166, F-3804, Grenoble, Cedex 9, France
[2] *Research Center for Quantum Communication Engineering*
at Department of Communication Engineering
Holon Academic Institute of Technology, 52 Golomb St., Holon 58102, Israel
[3] *Department of Mathematics and Physics,*
Faculty of Science and Science Education,
University of Haifa - Oranim, Tivon 36006, Israel
[*] *Corresponding author: nathan.logoboy@grenoble.cnrs.fr*
Received 20 October 2004, accepted 4 November 2004

Abstract

The existence of magnetic domains in non-ferromagnetic metals at quantizing magnetic fields is examined under conditions of de Haas-van Alphen oscillations in the range of strong magnetic fields and low temperatures in thin slabs for a three-dimensional electron gas. Dynamics of Condon domain walls are studied in bulk metals and films at time-independent and time-varying applied magnetic fields. Domain wall resonance and relaxation effects are considered. The influence of temperature, magnetic field, impurities and sample size on the width, velocity and mobility of domain walls is calculated. Magnons of a non-spin nature are defined and discussed. It is shown that the magnetic induction splitting in the sample due to the existence of the domain stripe structure changes the distribution of magnetic field in vacuum above the surface of the sample. Detection of these changes by Hall probes can give information about spatial configuration of the Condom domain structure.

PACS: 71.10 Ca; 71.70 Di

1 Introduction

Oscillations of thermodynamic quantities in an external magnetic field are the result of the oscillations of the density of states caused by the magnetic field quantization of the energy levels (Landau quantization) [1]. Many properties of electron gas in normal metals are periodic functions of magnetic fields as successive Landau levels sweep through the Fermi level due to an increase of the external magnetic field – for instance, oscillations of magnetization (de Haas-van Alphen effect- dHvA) [1]. The magnetic field changes the density of states and, consequently, the internal energy of the electron gas. Thus, when $\chi_B = \partial M/\partial B > 1/4\pi$ (M is the oscillatory part of the magnetization, B is the magnetic induction), the "realignment" of the density of states, connected with the change of magnetic induction B occurring during the stratification into phases, becomes energetically "convenient", and results in formation of Condon domains [1, 2]. This instability, caused by strong correlation of conduction electrons, is known as diamagnetic phase transition (DPT) [2]. The transformation occurs in each cycle of dHvA oscillations when the reduced amplitude of oscillations approaches unity [1]. A series of phase transitions takes place at discrete values of the external magnetic field H_{ex}. The reason for this collective effect is that an electron is subject to the magnetic induction B instead of the magnetic field H (the Shoenberg effect) [1]. Thus, an applied magnetic field H_{ex} of a few Tesla may "magnetize" non-magnetic metals in the sense of the appearance of magnetic domains. Condon domains were predicted by Condon in Ref. [3] and discovered in silver (Ag) by means of nuclear magnetic resonance (NMR) [4] and in beryllium (Be) and white tin (Sn) by means of muon spin-rotation spectroscopy (μSR) [5–9]. Domain formation at DPT was studied theoretically in [2, 3, and 10–20]. The DPT in the single-domain case for three-dimensional (3D) metals was described in [21–23]. The temperature dependence of the magnetic induction bifurcation due to the Condon domains was satisfactory reproduced in quasi-two-dimensional (2D) [24] and 3D metals [25]. It was shown that the temperature dependence of the magnetic induction bifurcation due to the Condon domains has a universal character and does not depend on the dimensionality of electron gas. The latter circumstance confirms the long-range nature of magnetic interactions between orbital magnetic moments of conduction electrons in metals under high (quantizing) magnetic fields [26], and evidences in favour of using the mean-field approach for the description of DPT.

Condon domains in a 3D electron gas are the only type of magnetic domains, for which the dynamics of domain walls (DW) has not been con-

sidered so far. However, for a 2D electron gas the oscillations of Condon DW were considered in [19] by analogy with ferromagnets. The motivation for the investigation of the DW dynamics of Condon domains is driven by interest in understanding the characteristic magnetic lengths of the system, deriving from the domain dynamics, and their comparison with parameters calculated from the static properties. The DW motion is determined by the fundamental nature of the magnetic material. Both theoretical and experimental investigations of the domain dynamics will give the characteristic sizes of domains and DW, and hence clarify the underlying physics of magnetic ordering phenomena under conditions of magnetic oscillations. Consequently, the dynamics of Condon DW should be studied as an additional tool for the investigation of the phenomenon.

Ordered states, such as Condon domains, should exhibit several kinds of dynamics: magnetization density waves (or magnons of a non-spin nature) [10] and DW motion. In weak magnetic fields the wall-displacement processes of ferromagnetic domains [27] govern the magnetization changes. The Condon DW should have a characteristic frequency of oscillations, so far unknown in 3D metals. Consequently, there should be a resonance dispersion of magnetic susceptibility, caused by wall displacement processes. Numerous observations have detected the above resonance behaviour in ferromagnets and ferroelectrics [28–31] and have furnished experimental evidence of the existence of DW mass. Thus, two types of domain dynamics experiments have been done, which provide the most part of the basis for the theoretical picture of DW motion [28, 31]. Small-motion or susceptibility studies mentioned above, are the first type, and large-motion or velocity versus applied field, are the second. The latter process is DW motion, which leads to reorientation or switching of the magnetization in domains, induced by an applied magnetic field. The above research of Condon domains dynamics deals with bulk metals.

The problem of the DW dynamics in thin films remains open and merits investigation as well. It would be useful to examine the dynamics of DW in 3D metals, where Condon domains have been detected experimentally. The dynamics of the interphase boundaries at first-order DPT was theoretically considered in [12] and [16]. It would be a mistake to identify the two types of the boundary motion, namely the interphase boundary and DW motion. We shall discuss this problem in Sect. 3.

The goal of this research of the Condon domain phase and DPT is the description of the dynamics of Condon DWs of the two above-mentioned types. To the best of our knowledge, all the theoretical and experimental studies of DPT and Condon domains have been focused on large samples,

and all the phenomena have been investigated on a macroscopic scale. Some static mesoscopic properties of metals undergoing DPT or containing Condon domains have been studied in [32].

In this paper we present a mean-field theory elaboration considering the bulk and size-dependent static and dynamic effects in the Condon domain phase. In a more general aspect the Condon "magnetism" has been recently surveyed in [33].

The paper is organized as follows. Section 1 is an introduction. Section 2 deals with the model of Lifshitz-Kosevich-Shoenberg including the Landau-type expansion of the thermodynamic potential density in the bulk and slab cases. Section 3 concerns the overdamped motion of DWs and the inertia effect on the DW motion. Section 4 refers to the finite-size effect on the motion of DW. Section 5 is devoted to DW resonance and relaxation. Section 6 discusses non-spin magnons. In Section 7 we concentrate on phase diagrams and dynamics of DW in gold (Au). In Section 8 we consider the stripe domain structure and calculate the periodic (along the normal to the DW plane) magnetic splitting due to Condon domains on the surface of the sample as a function of the distance between the surface and a possible position of the Hall probe in air. The measurements by means of Hall probe will provide us with the characteristic magnetic size, the domain size, and can be used for domain mapping on the sample of that surface. In this section a method for the velocity and mobility measurement of DWs is discussed. Section 9 is conclusions. Section 10 contains acknowledgements.

2 Model

The oscillator part of the thermodynamic potential density can be written neglecting all harmonics in the Lifschitz-Kosevich formula, but one, in the first harmonic approximation [1, 34]:

$$\Omega = \frac{1}{4\pi k^2}\left[a\cos\left(b\right) + \frac{1}{2}a^2(1-n)\sin^2\left(b\right)\right], \tag{1}$$

H is the magnetic field inside the material

$$b = k(B-H) = k\left[h_{ex} + 4\pi\left(1-n\right)M\right],$$

$k = \dfrac{2\pi F}{H^2}$, F is the fundamental oscillation frequency, $h_{ex} = H_{ex} - H$, is the small increment of the magnetic field H and the external magnetic field H_{ex}, n is the demagnetization factor; all the components of vectors are taken along

the direction of the magnetic induction. In the first harmonic approximation the magnetization is found from the implicit equation of state [1]:

$$4\pi kM = a \sin\left[k\left(h_{ex} + 4\pi\left(1-n\right)M\right)\right], \tag{2}$$

a is the reduced amplitude of oscillations: $a = 4\pi kA = 4\pi\left(\partial M/\partial B\right)_{B=H}$ [1], A is the first harmonic amplitude. If the magnetic interaction is strong enough, a state of lower thermodynamic potential can be achieved over part of an oscillation cycle by the sample breaking up into domains, for which the local value of magnetization alternates in sign from one domain to another. In the vicinity of the DPT temperature (found from the equation $a(T_c, H) = 1$) we can present the thermodynamic potential per unit volume as an expansion in powers of magnetization:

$$\Omega = 2\pi\left(1-a\right)M^2 + \frac{8}{3}\pi^3 k^2 M^4. \tag{3}$$

Accordingly, we arrived at the Landau-type thermodynamic potential density [21]:

$$\Omega = -\frac{A}{2}M^2 + \frac{B}{4}M^4, \tag{4}$$

where $A = 4\pi(a-1), B = (32/3)\,\pi^3 k^2$. In the case of the breaking up into domains, these equations are valid over the range of domain existence in the dHvA cycle. According to [34], the temperature and field dependence of the amplitude is

$$a\left(T, H\right) = a_0\left(H\right)\frac{\lambda T}{\sinh\left(\lambda T\right)}\exp\left[\,-\lambda\left(H\right)T_D\right], \tag{5}$$

$\lambda \equiv \dfrac{2\pi^2 k_B m_c c}{e\hbar H}$, m_c is the cyclotron mass. The limiting amplitude $a_0\left(H\right) \equiv a\left(\lambda T \to 0, H\right)$ is the combination of temperature-independent factors in the Lifschitz-Kosevich formula [34] - $a_0 = \left(H_m/H\right)^{3/2}$, k_B is the Boltzmann constant, e is the absolute value of the electron charge, c is the light velocity, $\hbar$ is the Planck constant, T_D is the Dingle temperature and H_m is the limiting field above which DPT does not occur at any temperature (it depends on the shape of the Fermi surface – see details in [15]). To construct temperature-magnetic field phase diagrams giving the range of the appearance of DPT [15] we use, henceforward, the implicit equation for the DPT temperature, putting (5) equals unity at the phase transition. At $a < 1$ $(T > T_c)$ the homogeneous phase exists with zero magnetization. At $a > 1$ $(T < T_c)$ the "magnetic", ordered phase appears with non-zero magnetization. The phase

transition of the second order with the well-defined transition temperature T_c takes place only at discrete values of magnetic induction. The envelope of these points serves as the DPT boundary. The left wing of the bell-shaped phase diagram corresponds to comparatively low magnetic fields: $\lambda T_c >> 1$, the right side corresponds to comparatively high magnetic fields $\lambda T_c << 1$. In the first case the DPT temperature in a slab, T_s, is given by [32]:

$$T_s = T_c \left[1 - \frac{3^{4/3}}{2^{2/3} \lambda T_c} \left(\frac{r_c}{L} \right)^{2/3} \right], \tag{6}$$

where r_c is the cyclotron radius and L is the slab thickness. Here T_c is the bulk DPT temperature. Based on the approach used in [32], one can derive T_s for high magnetic fields, $\lambda T_c << 1$,

$$T_s = T_c \left[1 - \frac{3^{7/3}}{2^{2/3} (\lambda T_c)^2} \left(\frac{r_c}{L} \right)^{2/3} \right]. \tag{7}$$

The question of what the bulk is, should be answered here, depending on the value of the second term in the brackets. If its contribution is negligible compared with unity, the phase transition temperature is size-independent, and the properties of the sample are considered as the bulk ones. In the opposite case the slab properties differ from those of the bulk sample. The size dependence of the DPT temperature in the slab is the strongest in Eq. (7), since, in contrast to Eq. (6), the second term in the brackets is comparable to unity, provided the factors λT_c and r_c/L are small. The cyclotron radius is always much smaller than the slab thickness, and the condition $\lambda T_c << 1$ is fulfilled at high magnetic fields corresponding to the right side of the $T-H$ bulk phase diagram. Then suppression of the ordered state is more easily realized in the case of (7) than in the case of (6). Using (7) and putting $T_s = 0$, we get that the sample reaches the minimal value of thickness $L_{\min}$: $L_{\min} = \frac{27\sqrt{3}}{2} r_c \, (\lambda T_c)^{-3}$.

Therefore, the size dependence of the A - coefficient is related to DPT point shift to lower temperatures at small sizes. The size, at which the magnetic ordering becomes unstable, is the critical size. Accordingly, at the critical sizes, a balance among the volume, surface and gradient energies determines a characteristic phase transition point ($T_s < T_c$), i.e. a new phase transition point, instead of the original bulk phase transition point T_c. Beyond this transition temperature the ordered phase will be suppressed in the sample with the dimensions less than the critical sizes. This process is analogous to the classical homogeneous nucleation process, where the

condensed phase nuclei are not stable unless the radii of the condensed phase nuclei are larger than a specific critical size.

3 Dynamics of domain walls

3.1 Overdamped motion

Eq. (3) is valid in the centre of the period of magnetic oscillations ($h = 0$). This means that the sample is in the centre of the oscillation cycle, so that the up and down domains are equally wide. In the case of stationary motion of the DW acted upon by an "external force", an external magnetic field h removes the equivalence of the states to the right and left of the DW. When $h \neq 0$ and it varies, the energy balance is altered and rearrangements of the domain structure take place, mainly through the motion of DWs. Wall motion is the dominant magnetization mechanism. The DW will move in such a way that the volume of energetically favourable domains increases at the expense of energetically unfavourable ones. Thus, we consider the forced motion of the DW under the driving force h. Taking into account the declination from the centre of the period of oscillations and the energy of DWs, we should add the following two terms to thermodynamic potential density (4): $-hM + \frac{K}{2}(\partial M/\partial x)^2$, where $K = \dfrac{r_c}{4}$ is the inhomogeneity coefficient. Using the time-dependent Ginzburg-Landau equation $\dfrac{\partial M}{\partial t} = -\Gamma \dfrac{\partial \Omega}{\partial M}$ for the overdamped motion of DWs, we obtain the following equation:

$$\frac{\partial M}{\partial t} = \Gamma(K\frac{\partial^2 M}{\partial x^2} + AM - BM^3 + h), \tag{8}$$

Γ is the Landau-Khalatnikov transport coefficient. By using the time-dependent Ginzburg-Landau equation we say that the local rate of displacement of the order parameter is linearly proportional to the local thermodynamic force presented by the functional derivative of the thermodynamic potential density.The constant of proportionality, the kinetic coefficient Γ, is the response coefficient, which defines a time scale for the system. Therefore, we suppose that the DW dynamics has a relaxational character. This approach was used for the description of motion of interphase boundaries at the first-order DPT under temperature changes [12]. However, we also apply it to the motion of DWs. One of the reasons for its application was actually shown in [16]. Close to the first-order phase transition the so-called wetting of a DW occurs: the DW splits into two interphase boundaries between

the homogeneous phase and the "domain-up" and "domain-down", respectively. The shape of the interphase boundary coincides with that obtained in [12]. By "domain-up" and "domain-down" we understand two values of magnetization of opposite directions. This is the wetting of the DW by the homogeneous phase. The change from non-wetting to wetting behaviour occurs under well-defined conditions corresponding to attaining thermodynamic coexistence of the phase involved. The wetting of an interface by a solid phase may occur, when it becomes energetically favourable to insert a thin layer of a new phase at the interface. This condition can often be met when two phases are unstable, as in the vicinity of a critical or a triple point at first-order phase transitions. Comparison of the interphase boundary profile [16] with that obtained in [12] shows that the interphase boundaries formed by the wetting are kink-solitons of the time-dependent Ginzburg-Landau equation describing the interphase boundary between each of the two domains and the homogeneous phase. Since the interphase boundary and the domain boundary appear in the framework of this approach, we also use it here for DW motion induced by magnetic field.

Passing to the moving frame, $s = x - vt$, where v is the velocity in the direction x, we obtain

$$K\frac{d^2M}{ds^2} + (v/\Gamma)\frac{dM}{ds} + AM - BM^3 + ah = 0. \tag{9}$$

The solution of Eq.(9) corresponding to the DW boundary conditions is known [35]

$$M(s) = M_2 + \frac{M_1 - M_2}{1 + \exp(s/\Delta)}. \tag{10}$$

M_1, M_2 and M_3 are the roots of the equation $BM_3 - AM - ah = 0$:

$$\begin{aligned} M_1 &= \tfrac{1}{k\pi}\left(\tfrac{a-1}{2a}\right)^{1/2}\cos\left(\tfrac{\varphi}{3}\right), \\ M_2 &= \tfrac{1}{k\pi}\left(\tfrac{a-1}{2a}\right)^{1/2}\cos\left(\tfrac{\pi-\varphi}{3}\right), \\ M_3 &= \tfrac{1}{k\pi}\left(\tfrac{a-1}{2a}\right)^{1/2}\cos\left(\tfrac{\pi+\varphi}{3}\right), \\ \varphi &= \arccos\left(\tfrac{h}{h_m}\right), \\ h_m &= \tfrac{1}{3k}[2(a-1)]^{3/2}. \end{aligned} \tag{11}$$

M_1 and M_2 are the magnetization values in two domains corresponding to the two minima of the thermodynamic potential density (4) in an applied magnetic field, while M_3 is the saddle point of the thermodynamic potential density. The solution (10) is a kink-soliton corresponding to a large amplitude disturbance connecting two magnetization states by a single DW. At

h_m the magnetization has only one direction. Thus, the kink solution (10) describes the profile of the DW. The width Δ of this moving DW is equal to

$$\Delta = \frac{r_c}{4} \frac{1}{\left[2\pi \left(a-1\right)\right]^{1/2}}. \tag{12}$$

Its velocity is given by

$$v = \left(6\pi\right)^{1/2} \Gamma r_c \left(a-1\right)^{1/2} \cos\left(\frac{\pi+\varphi}{3}\right). \tag{13}$$

For $h << h_m$

$$v = \left(6\pi\right)^{1/2} \Gamma r_c \left(a-1\right)^{1/2} \sin\left(\frac{h}{3h_m}\right) \tag{14}$$

or, replacing the sine in (14) by its argument and using (11), we obtain

$$v = \frac{\left(3\pi\right)^{1/2} \Gamma r_c k h}{2\left(a-1\right)}. \tag{15}$$

Since h is small compared to the applied field inducing magnetic oscillations, we can, thus, justify the considered shape of the DW. The plane wall approximation is valid for small applied fields, where a small curvature lets to balance the forces tending to bend the DW.

Since the DWs do not move until the acting field nearly reaches a threshold magnetic field, below which the DW is pinned and above which the DW moves forward, the velocity in (15) is proportional to the excess magnetic field. This linear dependence is expected in the mean-field theory. The depinning threshold may be treated as a dynamic phase transition and analysed as a critical phenomenon.

The mobility of Condon DW μ can be determined as follow [36]:

$$\mu = \lim_{h \to 0} \left[\nu\left(h\right)/h\right]. \tag{16}$$

Hence,

$$\mu = \frac{\sqrt{3\pi}\Gamma r_c k}{2\left(a-1\right)}. \tag{17}$$

3.2 Inertial effect

DW resonances have not been subjected to any experimental investigations for Condon domains in the 3D electron gas. However, the existence of the DW mass can hardly be excluded from general arguments. To describe the rapid, non-overdamped, movement of the DW, the inertia term is added. It should include a product of the inertial factor m and the second time derivative of the magnetization $\frac{\partial^2 M}{\partial t^2}$. Then, in the moving frame the first term in the left side of Eq.(9) transforms into $K - mv^2$. In this case the DW width is given by

$$\Delta = \frac{r_c}{4} \frac{1}{\left\{2\pi\left(a-1\right)\left[1+24\pi m\Gamma^2\left(a-1\right)\cos^2\left(\frac{\pi+\varphi}{3}\right)\right]\right\}^{1/2}}. \qquad (18)$$

The influence of the inertial effect is determined by the dimensionless factor $m\Gamma^2$. Both factors, m and Γ, are parameters of the theory and should be extracted from the analysis of the system based on experiments. The connection between the inertial factor and the DW mass will be found in Section 7. When $m = 0$, Eq.(18) coincides with Eq.(12). The velocity of the DW is then given by

$$v = \frac{\sqrt{6\pi}\Gamma r_c \left(a-1\right)^{\frac{1}{2}} \cos\left(\frac{\pi+\varphi}{3}\right)}{\left[1+24\pi m\Gamma^2\left(a-1\right)\cos^2\left(\frac{\pi+\varphi}{3}\right)\right]^{1/2}}. \qquad (19)$$

Analogously, Eq. (19) transforms into (13), when $m = 0$. In case of $h << h_m$, Eqs. (18) and (19) give the expressions for the DW width

$$\Delta = \frac{r_c}{4\left[2\pi\left(a-1\right)\right]^{1/2}} \frac{1}{\left[1+\frac{3\pi\Gamma^2 m k^2 h^2}{\left(a-1\right)^2}\right]^{1/2}} \quad , \qquad (20)$$

and for the DW velocity

$$v = \frac{\sqrt{3\pi}\Gamma r_c k h}{2\left(a-1\right)} \frac{1}{\left[1+\frac{3\pi\Gamma^2 m k^2 h^2}{\left(a-1\right)^2}\right]^{1/2}}. \qquad (21)$$

If $m\Gamma^2 << 1$, the inertial effect seems to be negligible. If $m\Gamma^2 >> 1$, the inertial effect is substantial. The factor $(kh)^2$ is changed in the interval $0.01 - 1$ for reasonable values of temperature and magnetic field, and its influence on the dynamics of DWs is smaller than the influence of the factor $m\Gamma^2$. Eq. (21) exhibits critical temperature dependence in the overdamped

limit. The field dependence of the velocity of DWs (21) coincides with the one derived in [36] for the fast motion of DWs in ferromagnets. It is seen from (20) that the DW width narrows when the inertial factor increases.

Comparing (21) with the equation for the velocity of DWs measured in ferromagnets [35]

$$v = \frac{\mu h}{\left[1 + (\mu h / v_{_m})^2\right]^{1/2}}, \tag{22}$$

where v_m is the limiting velocity of the DW, we obtain a very simple formula: $v_m = (K/m)^{1/2}$. Thus, the limiting velocity v_m is determined by the ratio of the inhomogeneity and inertia coefficients. The limiting velocity is the velocity of the domain motion when the second term in the brackets in (21) and (22) is much larger than unity. It depends on temperature, magnetic field and the sample size and will be estimated in Section 7. The limiting velocity is derived in the absence of dissipation. In the second limiting case of the overdamped DW motion $m = 0$ and $v = \mu h$. It should be noted that the field mobility is unaffected by the inertial term. Eqs. (12), (18) and (20) are presented for $v << v_m$, otherwise the DW thickness decreases like $\left[1 - (\nu/\nu_m)^2\right]^{1/2}$ with the velocity increase.

4 Dynamics of domain walls and size-dependent effects

The results of Section 3 are valid for infinite samples. It is clear that sample sizes should be taken into account. Let us to consider a slab of infinite planar extent ($L_x, L_y \to \infty$) and of finite thickness L_z. We take into account the layer-like domain structure with a phase transition of the second order in the case of an 180^0 DW. We examine this sample geometry because all the direct measurements of Condon domains [3-9] were made for plate-like samples, when two dimensions of the specimen were much larger than its thickness. Using the results of Section 2, one can obtain equations for the dynamics of DWs in a slab of finite thickness.

The slab under consideration is a 3D spatial system, being infinite in two dimensions and confined in its thickness. Since the mean-field critical exponents obtained in the framework of Landau theory are not sensitive to the details of the microscopic system, they are universal [27]. Thus, the critical exponents calculated in the infinite sample are the same in the slab. This means that the size-finite renormalization of the reduced amplitude of

magnetic oscillations occurs as a result of the crossover from the bulk to the slab: $a \to \tilde{a}$, where $\tilde{a}$ is the reduced amplitude of dHvA oscillations taking into account the finite-size effect on the slab. Then, the width of the DW in the case of the overdamped motion is

$$\Delta = \frac{r_c}{4} \frac{1}{\left[2\pi \left(\tilde{a} - 1\right)\right]^{1/2}} \quad . \tag{23}$$

Close to the phase transition temperature, where

$$\left(\tilde{a} - 1\right) = \left(\frac{\partial a}{\partial T}\right)_{T=T_s} \left(T_s - T\right), \tag{24}$$

we obtain

$$\begin{aligned} \left(\frac{\partial a}{\partial T}\right)_{T=T_s} &= \frac{\lambda^2 T_s}{3}, \ \lambda T_s << 1, \\ \left(\frac{\partial a}{\partial T}\right)_{T=T_s} &= \lambda, \ \lambda T_s >> 1, \\ T_s &= T_c \left[1 - \left(\frac{L_{\min}}{L}\right)^{2/3}\right]. \end{aligned} \tag{25}$$

At thick slabs $\tilde{a} = a$, and the bulk properties, therefore, take place: $T_s = T_c$.

$$v = (6\pi)^{1/2} \Gamma r_c \left(\tilde{a} - 1\right)^{1/2} \cos\left(\frac{\pi + \varphi}{3}\right). \tag{26}$$

For $h << h_m$ the velocity is as follows:

$$v = (6\pi)^{1/2} \Gamma r_c \left(\tilde{a} - 1\right)^{1/2} \sin\left(\frac{h}{3h_m}\right), \tag{27}$$

or replacing $\sin\left(\frac{h}{3h_m}\right)$ by its argument $\frac{h}{3h_m}$, we obtain:

$$v = \frac{(3\pi)^{1/2} \Gamma r_c k h}{2\left(\tilde{a} - 1\right)}. \tag{28}$$

Eqs. (26) – (28) include the dependence of the velocity on the slab thickness L and, thus, describe the size-dependent dynamics of DWs in the overdamped motion.

5 Domain wall resonance and relaxation

We have considered large-motion, or the velocity versus applied field dynamics of Condon DWs. The second type of the dynamics of Condon DWs is a so-called small-motion case or oscillations of DWs in the presence of a small time-varying magnetic field. We consider this effect in the 3D case, while oscillations of Condon DWs in the 2D electron gas were studied in [19] by analogy with ferromagnets. It is convenient to analyse this subject by proceeding to a simple equation of motion for a 180^0 wall [28, 29]. The small-amplitude periodic motion of unit area of such a DW in an applied field is determined, as is that of a simple harmonic oscillator, by its effective mass m_w, viscous damping coefficient γ, and stiffness coefficient α. The pressure on the wall is $2M_0H$, where M_0 is the magnetization in the domain and H is the applied field parallel to the direction of magnetization. We may write, therefore,

$$m_w \frac{d^2x}{dt^2} + \gamma \frac{dx}{dt} + \alpha x = 2M_0 H, \tag{29}$$

as the equation of motion of unit area of a 180^0 DW for small displacements x from equilibrium. The viscous damping parameter γ measures the energy losses according to the motion of the DW. It is difficult to calculate the kinetic coefficient γ, since the damping mechanism is not completely clear. Eddy current damping of DW motion in magnetic metals is usually large, but the motion is also damped by magnetic relaxation mechanisms. Experimental evidence of the existence of DW mass was obtained in many materials [28, 29].

The presence of the DW mass leads to a DW resonance. A characteristic frequency of DW oscillations should be observed by measuring magnetic susceptibility caused by the wall-displacement processes. Solving Eq. (29) for the case of an alternative magnetic field $H = H_0 \exp(i\omega t)$, where ω is the frequency, we obtain the expression for susceptibility χ caused by the DW displacement [28, 29]

$$\chi(\omega) = \frac{\chi_0}{1 - \left(\frac{\omega}{\omega_0}\right)^2 + \frac{i\omega}{\gamma/m_w}} \quad , \tag{30}$$

where χ_0 is the susceptibility at $\omega = 0$ given by

$$\chi_0 = \frac{3(a-1)}{2\pi^2 k^2 D\alpha}, \tag{31}$$

D is the domain width. The frequency of the DW resonance [29] (of Condon domains) is given by

$$\omega_0 = \left(\frac{\alpha}{m_w}\right)^{1/2}. \tag{32}$$

As it is known [1], $4\pi\chi_0 = a$. Then

$$\omega_0 = \frac{1}{k}\left[\frac{6\,(a-1)}{\pi D a m_w}\right]^{1/2}. \tag{33}$$

Taking into account the size-dependent effect, we obtain

$$\omega_0 = \frac{1}{k}\left[\frac{6\,(\tilde{a}-1)}{\pi D a m_w}\right]^{1/2}. \tag{34}$$

Let us estimate this frequency under conditions of the experiment [4] in Ag: $H = 9\mathrm{T}$, $T = 1.4\mathrm{K}$, $a = 2.6$, $m_w = 4.7 \cdot 10^{-11}\mathrm{g{\cdot}cm^{-2}}$ (see below details of the calculation of m_w) using Eqs. (31) and (32). In this case the resonant frequency is: $\omega_0 = 1.2{\cdot}10^7\,\mathrm{sec}^{-1}$ corresponding to the real frequency of about 2MHz. The NMR frequency in Ag, at which the domains were observed, was equal to 18MHz [4]. The calculated resonant frequency may be, therefore, observable since the screening due to the skin effect occurs, so that the skin layer is much larger than the domain width.

At high amplitudes of impulse fields the wall motion becomes irreversible and the stiffness becomes independent of the wall position, i.e. the inertial and stiffness terms in (29) are negligible. Thus, $\gamma v = 2M_0 h$ in this case. Comparing this equation to Eq. (15) we obtain the equation giving the relation between Γ and γ:

$$\Gamma = \frac{2\,(a-1)^{3/2}}{\pi^{3/2} k^2 r_c \gamma}. \tag{35}$$

This limiting case corresponds, therefore, to the strongly damped case. The motion of the DW in metals may be overdamped, since eddy currents weaken inertial effects. The value of m_w/γ may be taken, for example, from magnetic-resonance experiments. It is usually derived from the resonance linewidth [29]. Using Eq. (35) we can present the expression for mobility as follows:

$$\mu = \frac{[3\,(a-1)]^{1/2}}{\pi k \gamma}. \tag{36}$$

In [37] the damping coefficient γ is calculated, provided eddy currents are the dominant mechanism of damping. In terms of our model this coefficient is given by:

$$\gamma = \frac{16AD}{\pi B \rho c^2}, \tag{37}$$

where ρ is the resistivity. For the data of the NMR experiment in Ag [4], using $\rho = 10^{-12}\Omega\cdot$m at helium temperatures for the residual resistivity ratio 10000, typical for pure silver samples [38], we obtain $\gamma = 1.2 \cdot 10^{-2}g\cdot$cm$^{-2}\cdot$ sec^{-1}. Inserting the calculated damping into (36) we obtain the value of mobility 150 cm$\cdot$ sec$^{-1}\cdot$G^{-1}. The mobility is sensitive to the sample purity especially through the resistivity. Using the data of [4] we get $v \approx 15$m/ sec. This value shows an order of magnitude of the DW velocity in silver by using the given resistivity and the experimental data of [4]. According to (36) and (37), the mobility tends to zero on approaching the phase transition temperature. This behaviour is characteristic of the eddy current nature of damping. In the case of the relaxation mechanism of damping the mobility strongly increases when the sample reaches the DPT temperature. This follows from (17). Such a substantial difference between the critical temperature dependence of the mobility of DWs in the two cases enables to clarify the role of different mechanisms of damping in the DW motion.

In our model the relation between the inertia factor and the DW mass is given by

$$m_w = \frac{1}{16\pi^2 k^2} m \frac{(a-1)}{\Delta} \quad . \tag{38}$$

Eq. (38) is the result of calculations of the kinetic energy density

$$\frac{1}{2} m \int \left(\frac{\partial M}{\partial t}\right)^2 dx = \frac{1}{32} m \frac{(a-1)}{\pi^2 k^2 \Delta} v^2, \tag{39}$$

which is equal to $\frac{1}{2} m_w v^2$. The calculation of (38) and (39) is based on the calculation of the difference between the energy of the moving DW and the energy of the DW at rest, which is equal to $\frac{1}{2} m_w v^2$.

The limiting velocity of the Condon DW v_m under conditions of the experiment [4] in Ag can be estimated by using $v_m = (K/m)^{1/2}$(see Section IV): $v_m =$ 100m/sec. In calculations of the resonant frequency and the DW mass, m_w is taken as $4.7 \cdot 10^{-11}$g/cm^2. This value is calculated following the known consideration of the domain wall inertia in conducting media [39] based on the data of the NMR experiment [4]. In our case the calculation, made according to [39], gives the following result:

$$m_w = \frac{\pi D^3 A}{3B\rho^2 c^4}. \tag{40}$$

The relaxation time $\tau = \gamma/\alpha$ is the time, with which the DW responds to changes of the external "force" $2M_0h$. If the DW response to the applied field is rapid, the inertial effects are negligible. At frequencies low enough compared to the DW resonant frequency, the motion of the DW is a simple relaxation process with the real and imaginary parts of the susceptibility

$$\chi'(\omega) = \chi_0 \frac{1}{1 + (\omega\tau)^2}, \tag{41}$$

$$\chi''(\omega) = \chi_0 \frac{\omega\tau}{1 + (\omega\tau)^2}. \tag{42}$$

The calculation of $\omega_0\tau$ gives $4\pi^{-2}\sqrt{3a}$. This expression is distinct from that derived in [19] for a 2D electron gas - $\sqrt{3/4\pi}$- and includes the reduced amplitude of dHvA oscillations a depending on temperature, magnetic field and size sample for a thin specimen. Based on the data [4], one can obtain $\omega_0\tau \propto 1$. The response type is therefore unclear. However, increasing the reduced amplitude may lead to $\omega_0\tau >> 1$ and provide the resonance response. In the opposite case $\omega_0\tau << 1$, which also may be reached by changing temperature and magnetic field, the eddy currents pattern appear to move along as though it was attached to the moving DW. Thus, the inertial effect is negligible, and the DW motion is overdamped. For this reason, the consideration in Section 3 is valid. In a sense, the relaxational character of the DW response is supported by the analysis of the helicon resonance in Al under conditions of the Condon domains appearance [40]. The softening of the helicon has been shown in [40] to happen owing to the occurrence of Condon domains. The growth of the helicon damping has been found related to the relaxational dynamics of DPTs [40]. It cannot be explained by the eddy currents induced by helicons. The characteristic helicon frequencies in [41] are several hundreds of Hz. From the data presented in [42], the frequency that makes oscillations of DWs possible is about 1MHz. It is much larger than the helicon frequency. This means that DW motion will not occur at least at frequencies smaller than 1MHz. This conclusion is clear from the conditions of the experiment, in which the wavelengths of the helicons are much larger than the domain width. Consequently, the damping of helicons observed in [41] is not caused by eddy currents induced by motion of the DWs in the oscillating field of helicons. The similar calculation of the frequency of oscillations of DWs in Be was made in [42]. The authors showed

that in Be DW motion will not occur until 20MHz. The similar result was actually observed in [4] in Ag, where the Larmor frequency, 18MHz, did not cause domain motion. The analysis of the helicon damping in Al showed a strong temperature increase exhibiting critical slowing down in the electron relaxation time [40]. This characterizes the overdamped dynamics of magnetically interacting electrons in Al. The response of the DWs apparently reflects the response of the collectivized electrons determining the Shoenberg effect. In Al it should evidently be of a relaxational type. However, this fact does not necessarily lead to conclusions about the relaxational dynamics of DW in other metals in which Condon domains occur. A generalized conclusion on the type of dynamics of DWs is not evident. The type of dynamics of DWs remains an open problem requiring further clarification.

6 Non-spin magnons

In each magnetic system divided into domains there are two ground state patterns of magnetization: small oscillation motions of magnetization in one domain and DWs displacements where magnetization flips from one domain to another. Thus, in addition to kink-soliton localized modes, as DWs, which are large amplitude solutions of the equation of motion (8), linear small amplitude, extended magnons should exist in the system. Magnons of this non-spin origin have not been considered so far. One can derive the dispersion relation for the orbital magnons in the following manner.

The equation of motion for the magnetization is

$$m\frac{\partial^2 M}{\partial t^2} + AM + BM^3 - K\frac{\partial^2 M}{\partial x^2} = 0. \tag{43}$$

In the small-amplitude limit, the plane waves

$$M = M_0 \sin\left(qx - \omega_q t + \theta\right) \tag{44}$$

are the solution to Eq. (43), where θ is the phase, with the dispersion relation

$$\omega_q^2 = \frac{|A|}{m} + v_m^2 q^2 \tag{45}$$

Here q *is* the wave number and $v_m = (K/m)^{1/2}$is the phase velocity. Eq. (45) gives a magnon mode, which presents small amplitude oscillations about ground state value M_0. These excitations given by Eq. (45) are magnons [45], but not spin waves. The dispersion relation is different from

that for the "classic" magnons [29] with its quadratic dependence on the wave number, but coincides with the dispersion law for magnons in so-called weak ferromagnets [36]. The rare-earth orthoferrites are an example of weak ferromagnets, in which the spontaneous magnetization is small and the energy associated with the demagnetizing fields is significantly lower than the characteristic energy of the other relativistic interactions, e.g., the magnetic anisotropy energy. The first term in the right-side of Eq. (45) has the meaning of magnon activation. Substituting the expression for $A = 4\pi\,(a-1)$ (see Eq. (4)) into Eq. (45), we have

$$\omega_q^2 = \frac{4\pi\,|a-1|}{m} + v_m^2 q^2. \tag{46}$$

Let us estimate the gap frequency in (45), (46), i.e. the activation frequency. Using the magnetic field and temperature values for the Ag sample in [4], we calculate the reduced amplitude of quantum oscillations and the wave number-independent part of the frequency. It is approximately equal to $5\cdot 10^8\,\mathrm{sec}^{-1}$. It corresponds approximately to the real frequency of 100MHz. The gap frequency lowers as the temperature or magnetic field changes lead to the phase transition temperature exhibiting the soft-mode type behaviour: $\omega\,(q=0) \propto |a-1|^{1/2}$. At the field and the Dingle temperature used in [4] we obtain the frequency $\omega \approx 10$MHz at $T = 2.47$K.

Eq. (43) has an additional solution of the hyperbolic tangent spatial profile, which is the DW pattern [43]. The excitation energy, required to produce this pattern, is localized in the DW. This kind of excitation is quite the opposite of magnon excitations, where the energy is distributed throughout the sample. It is apparent [44] that magnons are extended and DWs are localized. For $h << h_m$ the profile of the moving DW at $\Gamma = 0$ becomes $h/2A + (A/B)^{1/2}\tanh\left((x-\nu t)/2\Delta\right)$ instead of $(A/B)^{1/2}\tanh\left(x/2\Delta\right)$. This result is evident since the DW shape is preserved at low fields.

7 Magnetization reorientation in gold

To construct the $T-H$ phase diagrams in Au we put $a=1$ in (5) and plot the dependence of T on H [25].

The curves in Fig. 1 form the locus of points of DPT for different Dingle temperatures (from 0K to 1K), reflecting the degree of purity of the sample in Au: outside the bell-shape curve the homogeneous phase takes place, while the ordered phase is located inside the bell. The interphase curves separate the two phases. The range of existence of the ordered phase decreases with increasing the Dingle temperature. As we stated in Section 2,

the region of high magnetic fields in the phase diagram exhibits a more pronounced size-dependent effect. In this range of fields the bulk phase transition temperature is given by [22]

$$T_c = \frac{\left[6\left(a_0 \exp\left(-\lambda T_D\right) - 1\right)\right]^{1/2}}{\lambda}. \tag{47}$$

Thus, in this case the largest shift of the phase transition temperature should take place.

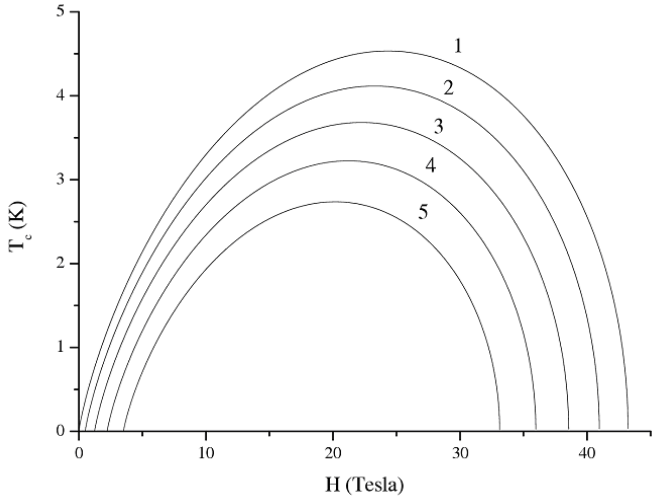

Figure 1: DPT diagrams in Au for different Dingle temperatures. The curve 1 denotes $T_D = 0$K, 2 – 0.25K, 3 –0.5K, 4 – 0.75K, 5 – 1K.

In Fig. 2 the DPT temperature in the slab $T_s\left(H\right)$ is shown as a function of the magnetic field value at zero Dingle temperature for different values of the slab thickness from 1μm to 8μm in Au. For constructing the plot, Eqs. (5), (6) and (7) are used. It is seen that the DPT temperature decreases with increasing the magnetic field value. The growth in the Dingle temperature leads to decreasing the phase transition temperature. The analytic results are obtained in two cases: comparatively low magnetic fields (6) and comparatively high magnetic fields (7). As it follows from this figure, the results are "sewn" and are seen to form the common bells-like phase diagram, also giving information about the range of parameter $\lambda T_c \propto 1$.

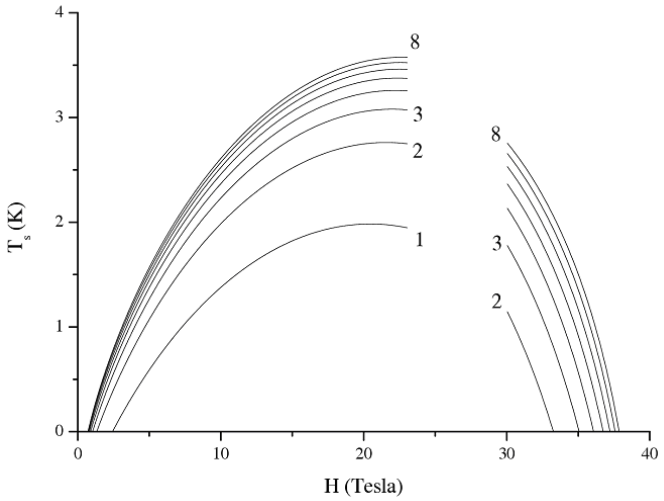

Figure 2: DPT temperature $T_s(H)$ in the slab as a function of the magnetic field at $T_D = 0.25$K in two cases: the left wing describes the region of comparatively low fields in the bulk phase diagram ($\lambda T_c >> 1$, where T_c is the bulk DPT temperature), the right wing describes the region of comparatively high fields in the bulk phase diagram ($\lambda T_c << 1$), at different values of the slab thickness from 1μm to 8μm in Au. The data in the two ranges are "sewn" and form the common bells-like phase diagram, also giving information about the range of intermediate values of parameter $\lambda T_c \propto 1$.

In Fig. 3 the DPT temperature $T_s(L)$ in the slab is presented as a function of the slab thickness for different Dingle temperatures from 0K to 0.5K in the region of high magnetic fields in Au. Eq. (7) is used for the plot construction. The graph is the phase diagram for a confined sample. Under the curves the range of the ordered phase is located for each Dingle temperature. The homogeneous phase is situated above and left of the curves. It is seen that the DPT temperature in the slab decreases with decrease of the slab thickness, reaching zero at a definite thickness. This minimum thickness $L_{\min}$ depends on the magnetic field and the Dingle temperature. The graph is plotted for high magnetic fields of the bulk phase diagram. Depending on the Dingle temperature, the DPT temperature in the slab reaches the bulk DPT temperature, starting from the slab thickness approximately equal to 100μm. Above this limiting value the sample properties are the bulk ones.

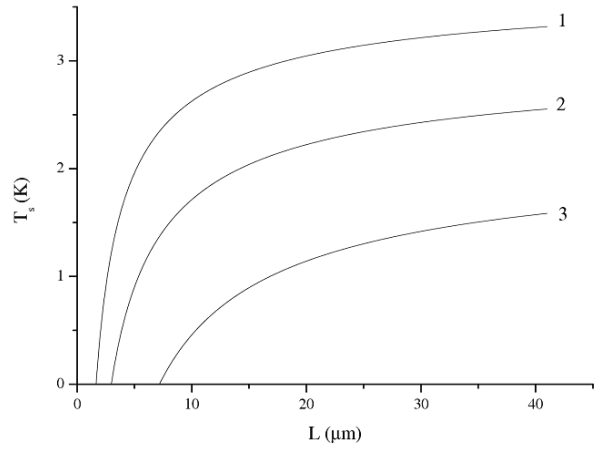

Figure 3: DPT temperature, $T_s\,(L)$, in the slab as a function of the slab thickness L. The DPT temperature is given at three different Dingle temperatures from 0K to 0.5K in the region of high magnetic fields in Au: 1 – 0K, 2 – 0.25K, 3 – 0.5K . For plotting the graph we used $H = 35$T.

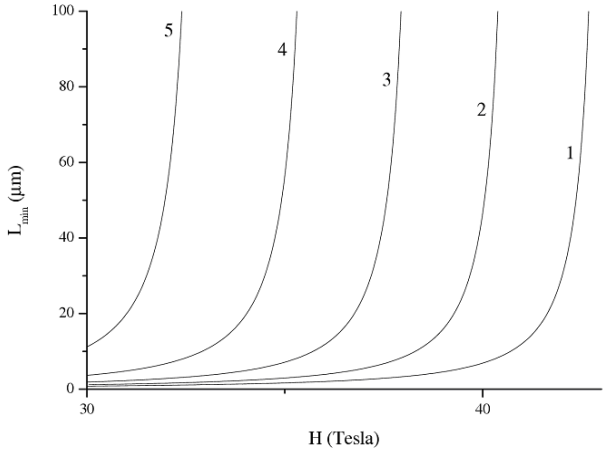

Figure 4: Magnetic field dependence of the minimal slab thickness $L_{\min}(H)$, in the case of strong magnetic fields and five different Dingle temperatures from 0K to 1K in Au: 1 – 0K, 2 – 0.25K, 3 – 0.5K, 4 – 0.75K, 5 – 1K.

Below this thickness the crossover occurs from the bulk size-independent properties to the finite-size ones.

In Fig. 4 the magnetic field dependence of the minimal slab thickness $L_{\min}$ is presented in the case of strong magnetic fields at different Dingle temperatures from 0K to 1K in Au. It increases with increasing of magnetic field. We use Eqs. (5) and (7) for the graph construction.

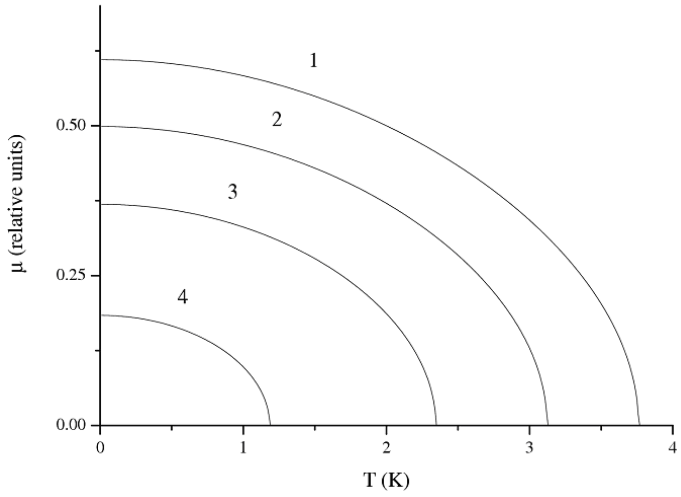

Figure 5: DWs mobility μ as a function of temperature T at $H = 35$T and different Dingle temperatures from 0K to 0.75K in Au: 1 – 0K, 2 – 0.25K, 3 – 0.5K, 4 – 0.75K. Mobility is given in units of $\sqrt{3}/(\pi k\gamma)$.

In Fig. 5 the DWs mobility μ is shown as a function of temperature at the magnetic field 35T and different Dingle temperatures from 0K to 0.75K in Au for bulk sample. Mobility is given in units of $\sqrt{3}/(\pi k\gamma)$. Eqs. (36), (24) and (25) are used for the calculation. The mobility increases as the temperature is lowered. It tends to zero at the DPT temperature, exhibiting the critical temperature dependence. The effect of critical slowing down takes place in the DW mobility.

In Fig. 6 the mobility μ is presented as a function of the slab thickness L at the value of magnetic field 35T, temperature 1K and different Dingle temperatures in Au. It is given in units of $\sqrt{3}/(\pi k\gamma)$. Eqs. (36), (24) and (25) are used for the calculation. Mobility decreases with decrease in the slab thickness tending to zero at the minimal thickness.

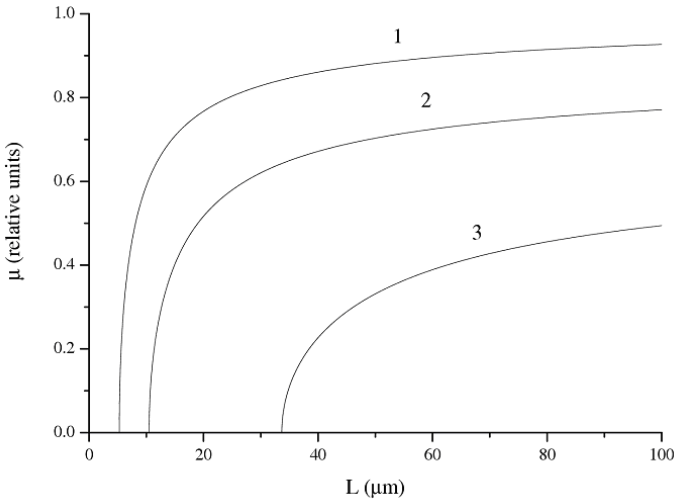

Figure 6: DWs mobility μ as a function of the slab thickness L at the magnetic field $H = 35T$, temperature $T = 1$K and different Dingle temperatures in Au: 1 – 0K, 2 – 0.25K, 3 – 0.5K. The mobility is given in units of $\sqrt{3}/(\pi k\gamma)$.

In Fig. 7 the $h-$dependence of the DWs velocity $v(h)$ is presented in units of the mobility μ in Au at the value of magnetic field 10T and temperature 1K for two Dingle temperatures: 0K – 1, 0.25K – 2, with the account of DW inertia. The velocity is given in units of h/h_m. Eqs. (19) and (11) are used for the calculation. Increase in the inertial effect leads to the change in the curvature of the graph indicating a tendency towards saturation in strong magnetic fields upon field increase. The curve shown in this figure is characteristic of inertia-response type systems. It is plotted at the values of magnetic field for which inertial effects are strong enough in comparing with damping resulting in saturation of the velocity with the field increase. The curves end when the reorientation is complete and the magnetization has only one direction. It is seen that the deterioration of sample purity, reflected in growth of the Dingle temperature, reduces the range of the domain existence, cutting the region of the allowed fields, at which the two-domain region takes place.

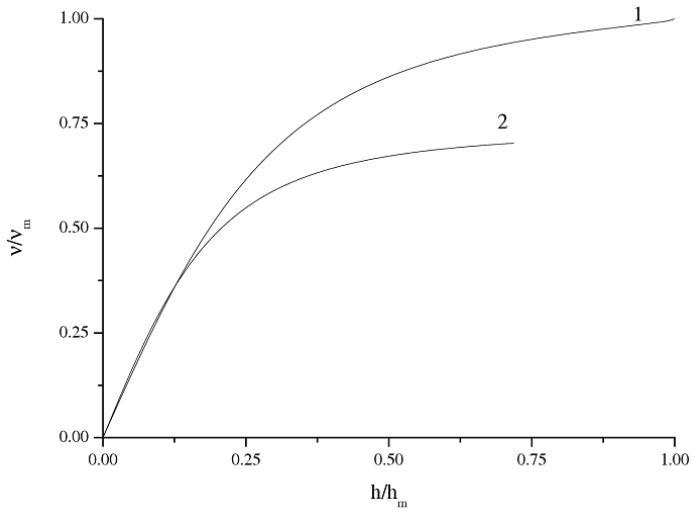

Figure 7: DWs velocity v in units of maximum velocity v_m as a function of the decrement of the magnetic field h (the deviation from the period centre of oscillations) at the magnetic field $H = 10$T, temperature $T = 1$K and two Dingle temperature: 1 – 0K, 2 – 0.25K , in Au in the case of inertial effects. The field h is measured in units of h_m. v_m is the limiting DWs velocity.

Since the temperature dependence of the resonant frequency coincides with that of mobility, the temperature and size curves of the frequency in relative units are similar to those presented in Figs. 5 and 6.

In Fig. 8 the magnon frequency ω is shown as a function of temperature T at the magnetic field 35T and different Dingle temperatures from 0K to 0.75K in Au. Frequency is given in units of $\omega_0 = (|A|/m)^{1/2}$. The frequency increases as the temperature is lowered. It tends to zero at the DPT temperature exhibiting the critical temperature dependence of the soft mode type. In contrast to the known mode softening occurring at structural and ferroelectric phase transitions, for which the soft mode frequency decreases according to $(T_c - T)^{1/2}$, in this case the magnon softening exhibits the temperature dependence $(a - 1)^{1/2}$. The latter formula is of a mean-field type: the order parameter is proportional to $(a - 1)^{1/2}$, approaching zero when the reduced amplitude a tends to unity. This bifurcation behaviour was detected in the domain phase in Be [6]. This temperature dependence of the frequency splitting in the domain phase in Be and Ag may evidence in favour of the soft mode appearance by analogy with the temperature behav-

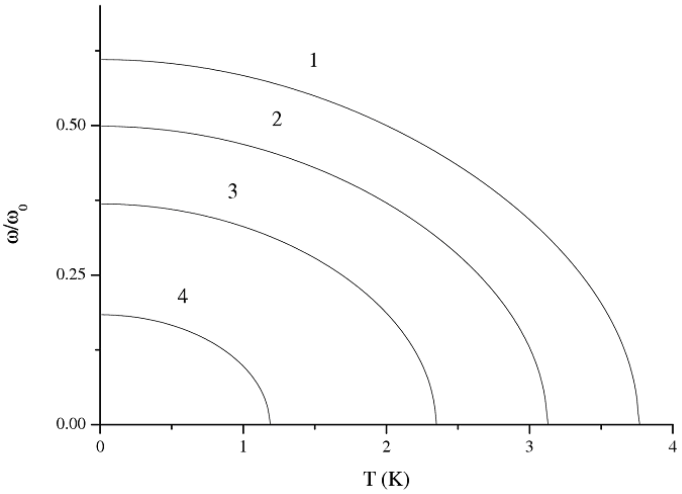

Figure 8: Magnon frequency ω as a function of temperature at the magnetic field $35T$ and different Dingle temperatures from 0K to 0.75K in Au: 1 – 0K, 2 – 0.25K, 3 – 0.5K, 4 – 0.75K. Frequency is given in units of ω_0.

ior of the frequency spectrum at structural, ferroelectric and ferromagnetic second-order phase transitions [26]. In the case of a continuous symmetry group, the low-frequency collective excitations, so-called soft modes, are present. In isotropic magnets spin magnon modes soften as temperature approaches the phase transition temperature from below.

In Fig. 9 the magnon frequency ω is presented as a function of the slab thickness L at different Dingle temperatures at the magnetic field 35T and temperature 1K in Au (Eqs. (46) and (7)). It is given in units of $\omega_0 = \sqrt{|A|/m}$. Frequency decreases with the decrease in the slab thickness, tending to zero at the minimal thickness. It is seen that the deterioration of sample purity, reflected in growth of the Dingle temperature, reduces the range of the domain existence, cutting the region of the allowed fields at which the two-domain region takes place.

The dispersion relation for the magnons of a non-spin origin is, therefore, obtained. At DPTs in bulk metals and confined metallic samples, the magnons softening with changing of temperature takes place.

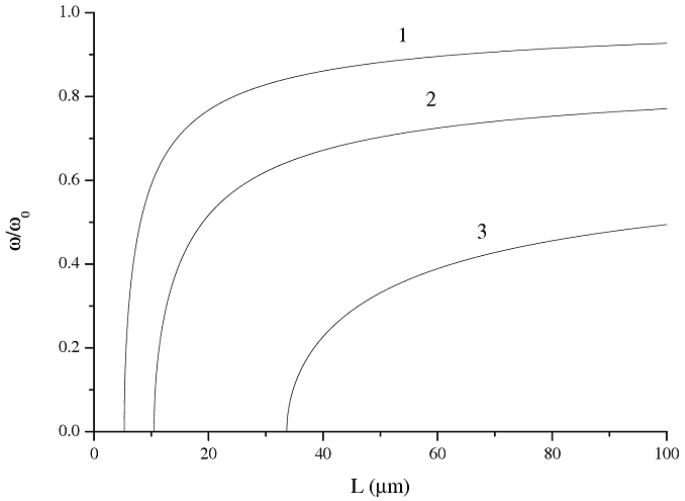

Figure 9: Magnon frequency, ω as a function of the slab thickness L at the magnetic field 35T, temperature 1K and different Dingle temperatures in Au: 1 – 0K, 2 – 0.25K, 3 – 0.5K. Frequency is given in units of ω_0.

8 Mapping of Condon domains

Magnetic domains in non-ferromagnetic metals, Condon domains, are of non-spin nature and present a rare example of the system, in which domain and domain wall sizes have not been measured so far. The knowledge of characteristic magnetic lengths could enable us to understand better the physics underlying this sort of instability of a 3D electron gas in normal metals. We have known only two characteristic dimensions of the system, i.e. the cyclotron radius r_c and the critical sample size L_c for the DPT existence (L_c is the film thickness, below which the order parameter of the DPT, i.e. the magnetization in each domain, is zero, see Fig. 9). For Ag we have calculated recently this critical size in [43], and for Au in the present paper. Thereby, we have shown that the Condon domain phase becomes unstable as the sample thickness L decreases. It occurs in the mesoscopic range. The non-uniform phase transforms to the uniform one at the critical size L_c. Hence, the phase transition temperature becomes zero at a finite value of the film thickness. It has been proven that the known theory of DPT is a limiting case of the finite-size theory [43]. However, the spatial domain structure, and especially the sizes of domains and DWs, as well as

the correlation length, determining the type of the ordering under study, have been unknown. Detection of the magnetic and correlation lengths of the system would enable us to gain an improved understanding of the spatial configuration of the Condon domain structure and to perform its imaging and mapping. The use of Hall probes, which are a very sensitive instrument for measuring magnetic fields, could shed light on the problem of the driving forces governing the onset of DPTs, and extract information on the characteristic range of these forces.

The main idea of the experiment on measurements of the characteristic magnetic lengths is based on the calculation of the magnetic induction splitting due to Condon domains on a surface of the sample as a function of the distance between the surface and a possible position of the Hall probe in air.

As it is known [1], the macroscopic characteristic magnetic lengths (domain and DW sizes) in the dHvA oscillations are governed by the considerations very similar to those in other domain situations. The last circumstance essentially simplifies these calculations. It should be noted that Condon domains, forming in the sample bulk, come to the specimen surface. In this sense, the situation in non-magnetic metals differs from ferromagnet samples on the surface of which, the closure domains usually appear, disturbing to find the bulk distribution of the domain structure, but resembles the picture of domain formation in the intermediate state in superconductors.

Let us consider the periodic stripe domain structure in a plate-like sample with the domain period $2D << L$, where L is the width of the plate (see, for example, [28, 44]). We assume that the surface of a crystal is parallel to the $x - y$ plane at $z = 0$, the external magnetic field H is parallel to z-axis and the domains with magnetization M along the $+z$ or $-z$ direction are separated by DWs lying parallel to the $y-z$ plane. For simplicity we assume that all domains have the same width D and the DWs are geometric ones, so that the DW width $\Delta << D$. The DWs are parallel to H, and we can neglect the contribution of magnetostatic energy at the boundaries between domains in comparing with the magnetostatic energy of the domains [1]. We characterise the given domain structure by magnetic induction splitting $\Delta B = B_1 - B_2 = 8\pi M$, where B_1 and B_2 are magnetic inductions in two adjacent Condon domains.

We calculate the spatial distribution of magnetic field above the sample $z > 0$ due to periodic (along the y-axis) induction splitting ΔB with the period $2D$ inside of the sample $z \leq 0$. The standard procedure based on

Maxwell's equations in magnetostatic approximation [44]

$$\text{div } \mathbf{B} = 0, \ \text{curl } \mathbf{H} = 0, \tag{48}$$

and boundary conditions, e.g., continuity of normal component of magnetic induction and continuity of tangential component of magnetic field, which in our case acquire the form

$$B_z\left(y, z = 0^-\right) = B_z\left(y, z = 0^+\right) \tag{49}$$

$$H_y\left(y, z = 0^-\right) = H_y\left(y, z = 0^-\right),$$

and enables us to obtain the following distribution of magnetic field above the surface of the sample ($z \geq 0$)

$$H_n = H_{ext} + \frac{1}{\pi}\Delta B \arctan \frac{\cos\left(\pi y/D\right)}{\sinh\left(\pi z/D\right)} \tag{50}$$

$$H_t = \frac{1}{\pi}\Delta B \text{Arcth} \frac{\sin\left(\pi y/D\right)}{\cosh\left(\pi z/D\right)} \tag{51}$$

where y is the direction parallel to the surface and perpendicular to the stripe domain structure, z is the direction normal to the surface, H_{ext} is the applied magnetic field, H_n is the field component normal to the surface, H_t is the tangential field component. The formulas (50)-(51) include the characteristic magnetic size, e.g. the domain size D. The graphical representations of H_z (50) and H_y (51) components of magnetic field to the surface of the sample are given in Figs. 10-13. To plot the figures we used the reduced values for components of magnetic field $\delta h_n = (2/\pi)\left(H_n - H_{ext}\right)/\Delta B$, $\delta h_t = (2/\pi)\left(H_t/\Delta B\right)$ and co-ordinates y=$y/2D$ and z=$z/2D$, respectively.

It follows from Eqs. (50)- (51) that the magnetic field close to the surface of the sample gives a map of the domains on the surface. Thus, the measurements of a magnetic field in several points outside the sample will give us the characteristic magnetic lengths of the system, and provide the deeper insight into underlying physics of magnetic ordering phenomena under conditions of magnetic oscillations.

The method of Hall probes may be effective for measurements of the dynamics of DWs, in particular useful for the measurement of their velocity and mobility. The main idea is as follows. When an applied magnetic field is perpendicular to the surface of the sample, the domains with preferable orientation start to grow, and those with unfavourable orientation start undergo narrowing. This effectively causes DWs to move, and eventually one

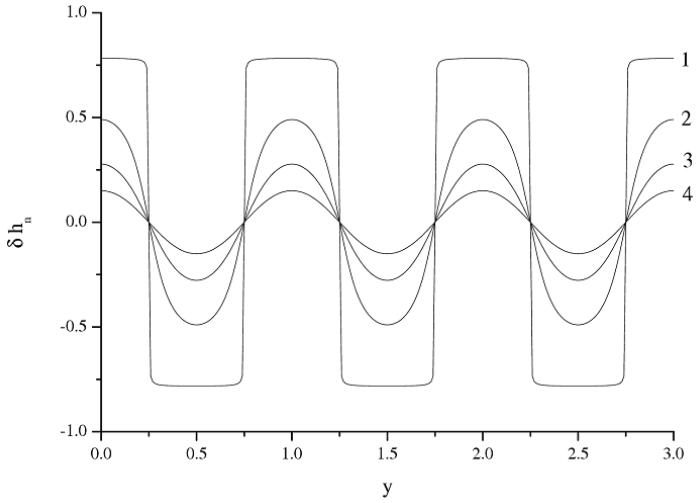

Figure 10: y-dependence of the reduced normal component of magnetic field δh_n at four different distances from the surface of the sample: 1 – z=0.01, 2 – z=0.1, 3 – z=0.2, 4 – z=0.3.

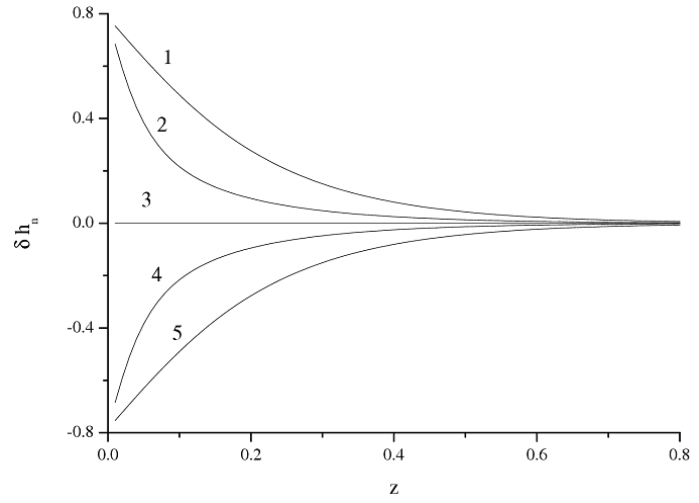

Figure 11: z-dependence of the reduced normal component of magnetic field δh_n at five different point on the surface of the sample: 1 – y=0, 2 – y=0.2, 3 – y=0.25, 4 – y=0.3, 5 – y=0.5.

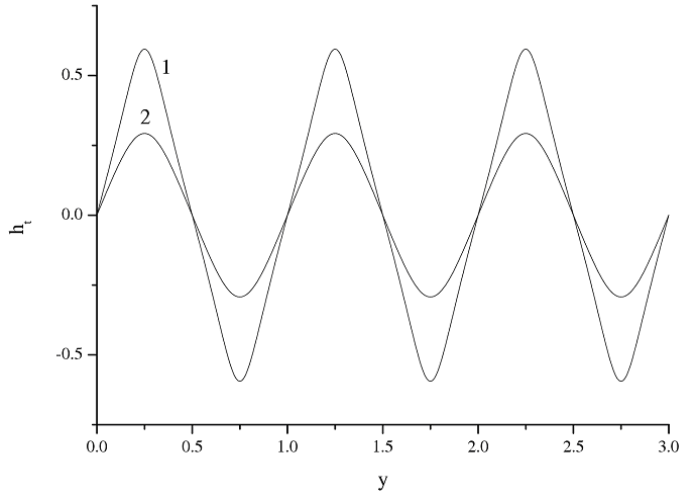

Figure 12: y-dependence of the reduced tangential component of magnetic field δh_t at two different distances from the surface of the sample: 1 – z=0.1, 2 – z=0.2.

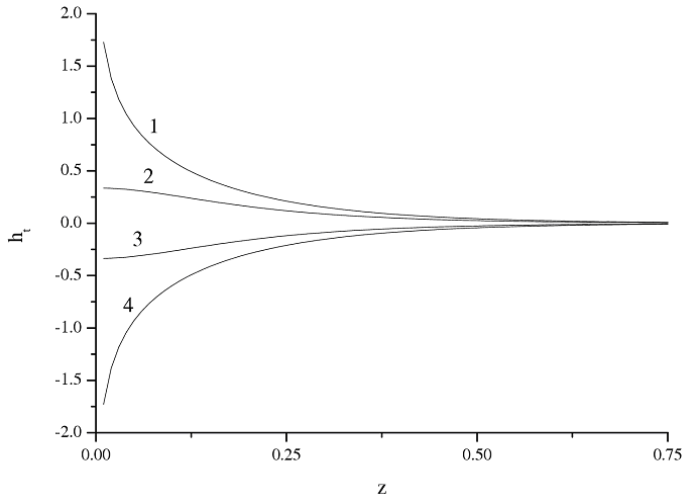

Figure 13: z-dependence of the reduced tangential component of magnetic field δh_t at four different points on the surface of the sample: 1 – y=0.25, 2 – y=0.4, 3 – y=0.6, 4 – z=0.75.

can get right underneath of the Hall probe. As the DW passes underneath the Hall probe, it changes the average magnetic field in the sensor area. Since the distance between different Hall probes is known and the passing time may be recorded, the velocity of DWs and their mobility can be measured by using Hall probes.

9 Conclusions

The finite-size effect on the DPT temperature is considered in high quantizing magnetic fields in a slab. Critical slab thickness, below which the magnetic ordering disappears, is found. The shift of the phase transition temperature towards lower temperatures is shown to be especially sensitive to the sample thickness in high magnetic fields corresponding to the right wing of the $T - H$ phase diagram.

Two types of DWs dynamic behaviour are studied. Large-motion, or velocity versus applied field, is the first type. Small-motion of DWs near the equilibrium state, exhibited in the dynamic susceptibility, is the second type. The overdamped motion of DWs is considered in the bulk and thin film cases. The inertia effect on the wall motion is also examined in the two cases. The mobility of DWs is derived and estimated. The characteristic frequency of DW oscillations under the alternative magnetic field application is calculated.

The dispersion relation for magnons of a non-spin origin is obtained. Temperature and sample size softening of the magnon mode of an orbital nature is considered in quantizing magnetic fields under conditions of the strong de Haas-van Alphen effect in bulk metals and confined metallic samples.

The distributions of magnetic field above the surface of the sample due to the inductance splitting in stripe domain structure are calculated. The possibility of Condon domain mapping and measuring of velocity and mobility of their walls is discussed.

We are indebted to I.D. Vagner, V. Egorov, R. Kramer, and I. Sheikin for useful discussions. We express our deep gratitude to P. Wyder for his interest in this work and his permanent inspiring influence on this field of research. One of us (A.G.) thanks the Center for Computational Mathematics and Scientific Computation of the University of Haifa for support. Some parts of this paper are reprinted with permissions from [A. Gordon, N. Logoboy, W. Joss, Phys. Rev. B **69**, 174417 (2004). Copyright (2004) by the American Physical Society] and from [A. Gordon, N. Logoboy, and

W. Joss, Solid State Comm. **130,** 131 (2004). Copyright (2004) by Elsevier Science Publishing House].

References

[1] D. Shoenberg, *Magnetic Oscillations in Metals* (Cambridge Univ. Press, Cambridge, 1984).

[2] A. Privorotskii, *Thermodynamic Theory of Domain Structures* (Wiley, N.Y., and Israel Univ. Press, Jerusalem, 1976).

[3] J.H. Condon, Phys. Rev. **45**, 526 (1966).

[4] J.H. Condon and R.E. Walstedt, Phys. Rev. Lett. **21**, 612 (1968).

[5] G. Solt, C. Baines, V.S. Egorov, D. Herlach, E. Krasnoperov, and U. Zimmermann, Phys. Rev. Lett. **76**, 2575 (1996).

[6] G. Solt, C. Baines,V.S. Egorov, D. Herlach, E. Krasnoperov, and U. Zimmermann, Hyperfine Interactions **104**, 257 (1997).

[7] G. Solt, C. Baines, V.S. Egorov, D. Herlach, E. Krasnoperov, and U. Zimmermann, Phys. Rev. B **59**, 6834 (1999).

[8] G. Solt, V.S. Egorov, C. Baines, D. Herlach, and U. Zimmermann, Phys. Rev. B **62**, R11933 (2000).

[9] G. Solt, C. Baines, V.S. Egorov, D. Herlach, and U. Zimmermann, J. Appl. Phys. **87**, 7144 (2000).

[10] S.C. Ying and J.J. Quinn, Phys. Rev. Lett. **22**, 231 (1969).

[11] A. Gordon and I.D. Vagner, J. Phys.: Cond. Matter **2**, 3787 (1990).

[12] A. Gordon, I.D. Vagner, and P.Wyder, Phys. Rev. B **41**, 658 (1990).

[13] A. Gordon, I.D. Vagner, and P.Wyder, Solid State Comm. **74**, 401 (1990).

[14] A. Gordon, B. Grushko, I.D. Vagner, and P. Wyder, Phys. Lett. A **160**, 315 (1991).

[15] B. Grushko, A. Gordon, I.D. Vagner, and P. Wyder, Phys. Rev. B **45**, 3119 (1992).

[16] A. Gordon, T. Salditt, I.D. Vagner, and P.Wyder, Phys. Rev. B **43**, 3775 (1991).

[17] M.A. Itskovsky, G.F. Kventsel, and T. Maniv, Phys. Rev. B **50**, 6779 (1994).

[18] I.D. Vagner, T. Maniv, and E. Ehrenfreund, Phys. Rev. Lett. **51**, 1700 (1983).

[19] R.S. Markiewicz, Phys. Rev. B **34**, 4172 (1986).

[20] T. Maniv and I.D. Vagner, Phys. Rev. B **41**, 2661 (1990).

[21] A. Gordon, M.A. Itskovsky, and P.Wyder, Phys. Rev. **B55**, 812 (1997).

[22] A. Gordon, M.A. Itskovsky, and P.Wyder, Solid State Comm. **103**, 167 (1997).

[23] A. Gordon, M.A. Itskovsky, and P.Wyder, J. Phys. Soc. Jap. **66**, 136 (1997).

[24] A. Gordon, M.A. Itskovsky, I.D. Vagner and P.Wyder, Phys. Rev. Lett. **81**, 2787 (1998).

[25] A. Gordon, M.A. Itskovsky, and P.Wyder, Phys. Rev. B **59**, 10864 (1999).

[26] S.C. Ying, B.J. McIntyre and J.J. Quinn, Phys. Rev. B **2**, 1801 (1970).

[27] L.D.Landau and E.M.Lifshitz, Phys.Z. Sowietunion **8**, 153 (1935) (English translation in: *Collective Works of L.D. Landau* (Pergamon Press, Oxford, 1965).

[28] A.P. Malozemoff and J.C. Slonczewski, *Magnetic Domain Walls in Bubble Materials* (Academic Press, N.Y., 1979).

[29] S.V. Vonsovskii, *Magnetism* (Wiley, N.Y., 1974).

[30] M.E. Lines and A.M. Glass, *Principles and Application of Ferroelectrics and Related Materials* (Clarendon, Oxford, 1977).

[31] B. Barbara, D. Gignoux and C. Vettier, *Lectures on Modern Magnetism* (Science Press, Beijing and Springer-Verlag, Berlin-Heidelberg, 1988).

[32] A. Gordon and P. Wyder, Phys. Rev. **64**, 224427 (2001).

[33] A. Gordon, I.D. Vagner, and P. Wyder, Adv. Physics **52**, 385 (2003).

[34] I.M. Lifshitz and A.M. Kosevich, Zh. Eksp. Teor. Fiz. **29**, 730 (1955) [Sov. Phys. JETP **2**, 236 (1956)].

[35] M.A. Collins, A. Blumen, J.F. Currie, and J. Ross, Phys. Rev. B **19**, 3630 (1979).

[36] V.G. Bar'yakhtar, B.A. Ivanov, and M.V. Chetkin, Usp. Fiz. Nauk **146**, 417 (1985) [Sov. Phys. Uspekhi **28**, 563 (1985)].

[37] H.J. Williams, W. Shockley, and C. Kittel, Phys. Rev. **80**, 1090 (1950).

[38] B.R. Barnard, A.D. Caplin, and M.N.B. Dalimin, J. Phys. F: Met. Phys. **12**, 719 (1982).

[39] W.J. Carr, Jr., AIP Conf. Proc. **34**, 108 (1976).

[40] A. Gordon, W. Joss, N. Logoboy, and I.D. Vagner, Physica B **337**, 303 (2003).

[41] V.I. Bozhko and E.P. Volskii, Pis'ma Zh. Eksp. Teor. Fiz. **26**, 337 (1977) [Sov. Phys. JETP Lett. **26**, 335 (1977)].

[42] L.R. Testardi and J.H. Condon, Phys. Rev. B **1**, 3928 (1969).

[43] A. Gordon, N. Logoboy, and W. Joss, Phys. Rev. B **69**, 174417 (2004).

[44] L.D. Landau, E.M. Lifshitz and L.P. Pitaevskii, *Electrodynamics of Continuous Media*, *Course of Theoretical Physics*, vol. **8** (Butterworth-Heinemann, Oxford, 2002).

[45] A. Gordon, N. Logoboy, and W. Joss, Solid State Comm. **130**, 131 (2004).